EPJ manuscript No.
(will be inserted by the editor)

Remarks on meson loop effects on quark models

I.K. Hammer[1], C. Hanhart[1], and A.V. Nefediev[2,3,4]

[1] Forschungszentrum Jülich, Institute for Advanced Simulation, Institut für Kernphysik and Jülich Center for Hadron Physics, D-52425 Jülich, Germany
[2] Institute for Theoretical and Experimental Physics, 117218, B.Cheremushkinskaya 25, Moscow, Russia
[3] National Research Nuclear University MEPhI, 115409, Kashirskoe highway 31, Moscow, Russia
[4] Moscow Institute of Physics and Technology, 141700, 9 Institutsky lane, Dolgoprudny, Moscow Region, Russia

arXiv:1607.06971v2 [hep-ph] 15 Nov 2016

Abstract. We investigate the effect of meson loops on the spectrum of quark states. We demonstrate that in general quark states do not tend to get very broad if their coupling to the continuum increases, but instead they decouple from the latter in the large coupling limit. We ascribe this effect to the essentially nonperturbative unitarization procedure involved. In the meantime, some quark resonances behave very differently and demonstrate collectivity in the sense that their pole trajectories span a wide, as compared to the level spacing, region therefore acquiring contributions from multiple bare poles rather than from the closest neighbors. While the actual calculations are done within particular, very simplified models, it is argued that the findings might well be general.

PACS. 11.55.Bq Analytic properties of S matrix – 12.39.-x Phenomenological quark models – 11.10.Gh Renormalization

1 Introduction

Quark models for strong interactions have a long history since the middle of the previous century when it was commonly accepted that hadrons were not elementary particles, and thus the idea of quarks as elementary building blocks was put forward. In its simplest form, quark models describe the confining interaction between effective constituent quarks which leads to the formation of hadrons as bound states. Such hadrons appear stable unless the model is "unquenched", that is, unless it incorporates a pair creation mechanism which enables strong decays. It was speculated then that, because of the large phase space available, the states high up in the spectrum acquire large widths and therefore they cannot be observed. In addition, hadronic loops, which bring an imaginary contribution to the mass of the state usually interpreted as width, also change the real part of the pole thus resulting in a hadronic shift—see, for example, Ref. [1] and references therein. In particular, in Ref. [1] a systematic approach to hadronic shifts was developed and a number of loop theorems was formulated and proved. On the other hand, it has been argued for a long time that when building quark models with coupled channels, unitarization cannot be neglected and even the appearance of extra, dynamically generated resonances is possible—see, for example, [2,3,4,5,6,7,8,9,10] and references therein. Furthermore, in a particular model, contrary to naive expectations, quark states may even become narrower as the coupling to the continuum grows [6,11].

In this paper we have a fresh look at the phenomenon of "unquenching". In particular, we discuss under which circumstances it is appropriate to treat the coupling to the continuum perturbatively and when large corrections from unitarization are to be expected. In this context it turns out that the real part of the hadronic loops plays a crucial role for the behavior of the pole trajectories. As these loops are divergent in an effective field theory their values must be fixed by some renormalization conditions that allow one to relate the strength of the real parts to observables. In the study we want to pursue here, aimed at an understanding of gross features that result from unitarization and not at a proper description of experimental data, we do not have such an option. Therefore we simply study the effect of different values for the real parts of the loops. Phenomenologically one may interpret this variation as studying different models, since each quark model generates its own vertex functions that in turn lead to specific real parts of hadronic loops. This will become evident from the discussion in Sec. 4.4.

While already in the famous work [12] and various later studies—for recent ones in the heavy quark sector we refer to Refs. [13,14,15]—unitarization effects are considered, to the best of our knowledge no detailed study of the effect of unitarization in the sense outlined above exists up to now. The goal of this study is to investigate systematically the effect of the coupling of a tower of quark states to a continuum channel in a unitary framework. For this we start from some model where the resonances are decoupled from the continuum. Then, the pole trajectories

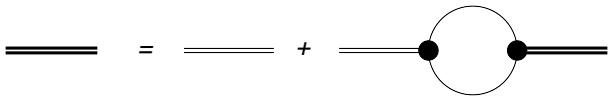

Fig. 1: Illustration of the Dyson equation: The physical Green's function is found from coupling individual quark states via meson loops. The thick double line denotes the physical Green's function while the thin double line denotes the bare quark model states. Single lines denote the particles of the continuum channel.

are followed as the coupling to the continuum channel is switched on and increased.

While being of interest on its own, this research may be viewed as a naive study of the QCD spectrum as the number of colors, N_c, gets reduced from some very large value [16,17] (for a pedagogical introduction to the large-N_c limit of QCD we refer to Ref. [18]). In the limit $N_c \to \infty$ the QCD spectrum comprises infinite towers of stable (with respect to strong interactions) hadrons, since the strength of three-point vertices scales as $1/\sqrt{N_c}$. At the same time the leading-order in N_c contribution to the mass of $\bar{q}q$ states turns out to be independent of the number of colors—fully in line with the general features of the model employed in this paper.[1]

2 Concept of modeling, important results and disclaimers

The main purpose of this research is to investigate in general terms the effect of hadronic loops on a spectrum of quark states. Thus, the models employed below are not intended to be used for realistic calculations of hadron properties as they are only meant to capture the gross features dictated by QCD. To be concrete, for the confinement potential we explicitly studied a linear as well as a quadratically rising potential. The resulting states are included in the s channel only. While performing each calculation with a fixed number of quark model states, N, we confirm that the general features of the pole trajectories do not depend on the number of basis states by repeating the calculation for different values of N, that even allows us to speculate about the $N \to \infty$ limit.

In this work the mentioned quark model states get coupled to each other via a meson loop in a single continuum channel. For the structure of the corresponding vertex functions again we use two different, simple models. The resulting Dyson equation for the physical Green's function is shown diagrammatically in Fig. 1.

[1] As explained in detail *e.g.* in Ref. [19], the large-N_c limit allows for deep insides into the nature of hadronic states. The approach we take here is complementary to that of Ref. [19]: while there the number of colors is increased from the starting point $N_c = 3$, here we model the effect of decreasing N_c from some very large value, admittedly with a much lower degree of rigor.

In our study the overall coupling strength for each resonance to the continuum channel is controlled by a single parameter that is varied for all quark states simultaneously. This procedure leads to certain pole trajectories, as a function of the mentioned strength parameter, that are studied for the different models mentioned above. For definiteness, the mass parameters in these calculations are chosen in a range that corresponds to $\bar{c}c$ states coupled to a pair of open-charm mesons. The most important findings of this work are:

- For small couplings each individual state located above a relevant threshold acquires a width that scales as the square of the coupling. The other states present in the system do not affect this behavior.
- As the coupling increases the width does not keep on growing for most of the states but, as soon as the self-energies get of the order of the level spacing, the pole trajectories bend and the widths decrease again. A typical shift of the real part of such a pole compared to its bare value is of the order of the level spacing, and the pole is therefore mostly influenced by the nearest neighbors.
- Besides the states just described at least one state in the spectrum behaves very differently. As the coupling increases, the trajectory of the corresponding pole is not bounded by the nearest neighbors but it covers several level spacings thus going far away from the original, bare pole position. As a result it is sensitive not only to its neighbors but also to remote states. For this reason we refer to such poles as to collective ones.
- Which state demonstrates this collective phenomenon and if this collectivity shows up in one or more states depends on the renormalization condition imposed and on the details of the model (type of the vertex function, number of states included, and so on).

Thus we found that in general, as soon as the coupling of quark states to the continuum gets large, unitarization effects cannot be neglected and they change severely the properties of the states. In particular, for large couplings there appear two types of states: ordinary and extraordinary states—this notion was introduced by Jaffe in Ref. [20]—which behave quite similarly for small couplings and are therefore indistinguishable in the weak coupling regime. Meanwhile, they behave quite differently as the coupling increases. In particular, for large couplings, the ordinary states tend to decouple from the continuum. Each of those states contains a prominent contribution from the original basis state and the admixture from other states decreases quickly with their distance to the pole. In the same limit, the extraordinary states demonstrate a collective phenomenon in the sense of sensitivity to multiple bare states, and it is this collectivity that could give us a clue on their physics as discussed in Sec. 5.

It should be stressed that the models we used are very simplified and by no means realistic. For example, we do not include t-channel exchanges of heavy mesons in the vertex dressing (as indicated in Fig. 2) — although formally they should be included — but just restrict ourselves to simplified models for the vertices whose struc-

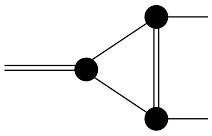

Fig. 2: Possible vertex dressing diagram *not* included in the present study. The meaning of the lines is the same as in Fig. 1.

tures are independent of the coupling strength. As was demonstrated in Ref. [21], the contribution of the triangle diagram from Fig. 2 is indeed suppressed in the weak-coupling regime ($g \to 0$). However, since the focus of this work is on qualitative studies of the behavior of the pole trajectories we dare neglect this diagram also for relatively large values of the coupling. A more refined study of the role played by the triangle diagram is left for future publications. We also do not allow for a t-channel exchange of light mesons in this work although the left-hand cuts they induce could lead to additional structure: while those will certainly change the quantitative behavior of the trajectories we do not expect the gross features to be changed. In addition, we only use a single continuum channel as well as a simplified form for the two-meson loop whose real part is controlled by just a single counter term. Still, regardless of those severe simplifications, since the two aforementioned types of states appear for all model versions we studied, we are tempted to claim the mentioned features to be general and therefore very likely to reveal themselves also in more realistic models. More refined studies will be presented in a subsequent publication.

3 Some instructive Examples

We start our presentation with a short discussion of systems with only one or two resonances where some features of the unitarization and regularization can already be discussed using simplified analytic calculations. In the subsequent Sections we turn to more general cases.

For simplicity we consider only one continuum channel, so that the Riemann surface consists of two sheets: the first (physical) sheet and the second (unphysical) sheet. Poles on the physical sheet are only allowed to reside on the real axis below the threshold and they correspond to bound states. The poles on the unphysical sheet located on the real axis below the threshold correspond to virtual states. All other poles on the second sheet correspond to resonances.

3.1 Single-resonance case

As the simplest example, we consider a single scalar resonance R coupled to a continuum channel $\varphi\bar{\varphi}$ with $\varphi(\bar{\varphi})$ being a scalar (anti)meson,

$$\mathcal{L} = \frac{1}{2}\left[(\partial_\mu\varphi)^2 - m^2\varphi^2\right] + \frac{1}{2}\left[(\partial_\mu\bar{\varphi})^2 - m^2\bar{\varphi}^2\right] + \frac{1}{2}(\partial_\mu R)^2 - \frac{1}{2}M^2R^2 + gR\bar{\varphi}\varphi. \quad (1)$$

The physical propagator of the resonance is calculated from the Dyson equation $G = G_0 - G_0\Sigma G$ with the solution

$$G = \frac{G_0}{1 + G_0\Sigma} = \frac{1}{s - M^2 + \Sigma}\ , \quad (2)$$

where $G_0 = 1/(s - M^2 + i0)$ is the bare scalar propagator, Σ is the selfenergy,

$$\Sigma = -g^2\Pi, \quad (3)$$

g is a real coupling constant, and $\Pi = \frac{1}{i}$ is the loop operator. If Π is treated as an energy-independent complex number then the pole of the dressed propagator (2) is located at $s_p = M^2 + g^2\Pi$. If now $\mathrm{Im}\Pi \neq 0$ then $|\mathrm{Im}(s_p)| \to \infty$ in the limit $g \to \infty$ that means that, for a constant selfenergy the width grows for an increasing coupling and it can become arbitrarily large.

In contrast to the toy example above, a more realistic selfenergy Σ is s-dependent. This is a necessary consequence of the analytic properties of the S matrix that require the presence of a pole at s_p^* if there is a pole at s_p. To proceed we need to specify the continuum channel for which we stick to the simplest two-body system formed by a scalar particle φ and its antiparticle $\bar{\varphi}$ which can interact only via the resonance R. To leading order in the center-of-mass momentum

$$k = \frac{1}{2}\sqrt{s - 4m^2}, \quad (4)$$

where m is the mass of the field φ, the selfenergy operator reads

$$\Pi(s) = -\frac{i}{16\pi m}k - \Delta(g). \quad (5)$$

The term $\Delta(g)$ is a real function which depends only on the masses and on the coupling constant g. The function $\Pi(s)$ is supposed to parametrize the leading energy dependence of the underlying loop function depicted in Fig. 1. Since this loop is divergent, as long as no form factors are introduced, some regularization procedure is required to fix its real part. Since in this exploratory study we cannot use experimental information to fix the real part of the loop, we study the impact of different values for $\Delta(g)$. Phenomenologically this means that we simulate in this way different quark models, since those will generate different hadronic form factors that in turn lead to different values for the real part of $\Pi(s)$. We come back to this discussion in Sec. 4.4.

Note that unitarity requires the spectral density

$$w(s) = -\frac{1}{\pi}\mathrm{Im}G(s) \quad (6)$$

to be normalized as

$$\mathcal{N} = \int_{s_{\rm th}^{\rm min}}^{\infty} w(s)ds = 1 - \sum_n Z_n, \tag{7}$$

where $s_{\rm th}^{\rm min} = (2m)^2$ is the lowest open threshold and the sum runs over all bound states (first sheet poles). Here Z_n denotes the corresponding wave function renormalization constants that may be interpreted as the probability to find the n-th bare state in the continuum wave function [22,23].[2] It is easy to verify that the spectral density constructed with the help of Eq. (2) is indeed normalized to unity for small couplings g for all values of the subtraction constant Δ. Meanwhile, as the coupling grows, for a particular sign of Δ, it happens that additional poles enter the physical Riemann sheet and turn into bound states. In this case the spectral density (6) is not normalized to unity any more, and the deviation of the normalization integral from unity is given by Eq. (7) with nonzero Z's. As before, this feature is independent of a particular choice of Δ.

Substituting function (5) into Eq. (2) it is straightforward to find the poles of the physical propagator,

$$s_p = M^2 - g^2\Delta - \frac{1}{8}\left(\frac{g^2}{16\pi m}\right)^2 \pm \frac{g^2}{32\pi m}\sqrt{4m^2 - M^2 + \frac{1}{8}\left(\frac{g^2}{16\pi m}\right)^2 + g^2\Delta}\,, \tag{8}$$

which depend on Δ.

As the first example we choose as renormalization condition the requirement that the real part of the pole studied does not move when the coupling to the continuum is switched on. This leads to the condition

$$\Delta(g) = -\frac{1}{8}\frac{g^2}{(16\pi m)^2}, \tag{9}$$

for which Eq. (8) for the poles position simplifies considerably to read

$$s_p = M^2 \pm \frac{1}{2}\left(\frac{g^2}{16\pi m}\right)\sqrt{4m^2 - M^2}. \tag{10}$$

For $M > 2m$ the square root in Eq. (10) is always imaginary and the width of the state R grows quadratically with g. This behavior is similar to the one for the constant Σ considered above, however now the unitarity condition $s_p^{(2)} = \left(s_p^{(1)}\right)^*$ is fulfilled automatically.

Alternatively we could have chosen the condition $\Delta(g) \equiv 0$, which implies that Δ is naively absorbed into a redefinition of the mass M. Then the poles position in the complex momentum plane—derived from Eq. (8)—reads

$$k_p = -\frac{i}{8}\left(\frac{g^2}{16\pi m}\right) \pm \frac{1}{2}\sqrt{M^2 - 4m^2 - \frac{1}{16}\left(\frac{g^2}{16\pi m}\right)^2}. \tag{11}$$

[2] For a recent discussion see, for example, Ref. [24].

In Fig. 3(a) we show the behavior of the poles k_p as a function of the coupling g for $M > 2m$. In the limit $g = 0$ there are two symmetric real poles which describe a stable quark state R. As g deviates from zero but remains small, $g^2 \ll 64\pi m\sqrt{M^2 - 4m^2}$, the state R acquires a small width and turns to a resonance. As g increases further, contrary to the naive expectations, the width does not grow infinitely, but the poles approach each other, they collide at the imaginary axis for $g^2 = 64\pi m\sqrt{M^2 - 4m^2}$, and then, for $g \to \infty$, one pole leaves the near-threshold region while the other one approaches the threshold from below. It is interesting to note that such asymmetrically located poles for near threshold states can be interpreted as a signature of a predominantly molecular nature of the state [25,26]. The underlying pole counting approach is in line with the famous compositeness criterion by Weinberg [27], as shown in Ref. [23].

The corresponding trajectories of the poles in the complex s-plane are shown in Fig. 3(b).[3] In particular, for $g = 0$ one has two degenerate poles lying on the real axis above threshold which then travel symmetrically in the second Riemann sheet until they collide again on the real axis below the threshold. Then, in agreement with the discussion of the poles in the complex k-plane, one of them leaves the near-threshold region while the other turns to a virtual state. It is easy to verify that the maximal imaginary part of the pole in the complex s-plane is $(M^2 - 4m^2)/4$. Therefore the state never gets arbitrarily broad and its maximal possible width is governed by the proximity of the bare poles to the threshold.

For $M < 2m$ one can choose a different renormalization scheme with

$$\Delta = \frac{1}{32\pi m}\sqrt{4m^2 - M^2}, \tag{12}$$

that ensures $\Sigma(s = M^2) = 0$ for any g, so that the bound-state pole stays fixed at $s = M^2$. Meanwhile, its counterpart on the unphysical Riemann sheet moves away from the threshold with a growing value of g. Thus the system behaves similarly to the previous case for large couplings.

3.2 Two-resonance case

Now we consider a system of two resonances, R_1 and R_2, which, as before, couple to a single elastic channel $\varphi\bar{\varphi}$. The resonances therefore communicate through the off-diagonal elements of the selfenergy operator

$$\Sigma_{ij} = -g_i g_j \Pi.$$

The poles of the scattering matrix in such a two-chanel problem come as solutions of the equation $\det(1 + G_0\Sigma) =$

[3] For a discussion of the pole trajectories from a different perspective we refer the reader to Ref. [28]. A detailed investigation of the interplay of quark and meson degrees of freedom in near-threshold resonances and the discussion of the resulting behavior of the poles can be found in refs. [29,30,31]. Coupled-channel dynamics of the poles describing near-threshold states can be found, for example, in Refs. [32,33,34].

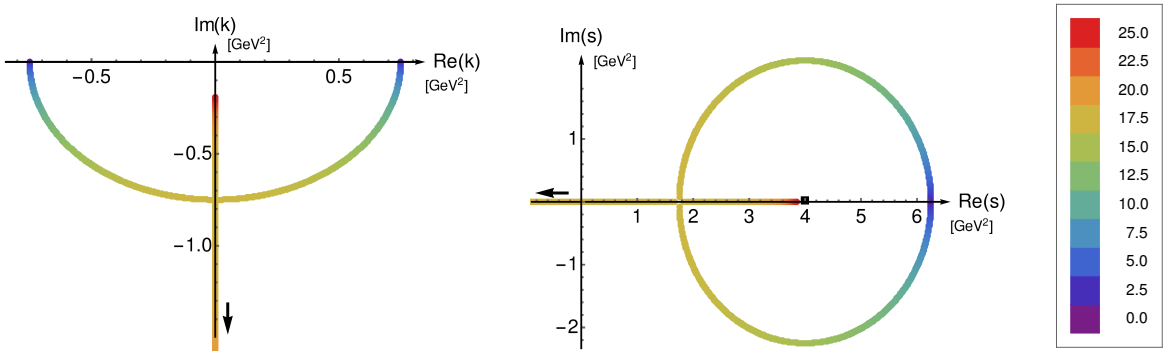

(a) (b)

Fig. 3: Pole trajectories for the renormalization condition $\Delta(g) = 0$ and for the values of g between 0 and 25 GeV ($M = 2.5$ GeV, $m = 1$ GeV). The left (right) panel shows the pole trajectories in k-plane (s-plane). The black square indicates the threshold.

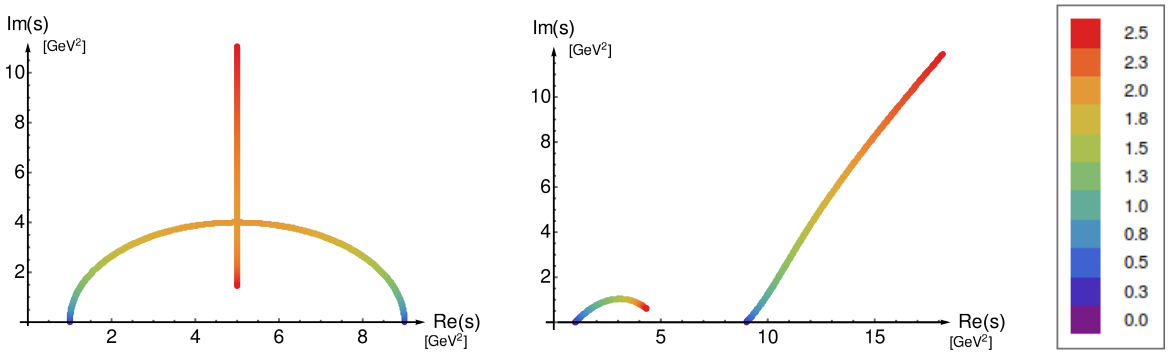

(a) (b)

Fig. 4: Pole trajectories in the upper half of the complex s-plane as given in Eq. (14) for g growing from 0 to 2.5 GeV (see Eq. (13) for the values of other parameters). The left(right) panel shows the result for $\Pi = i (\Pi = 1 + i)$.

0, where $G_0 = \mathrm{diag}((s - M_1^2 + i0)^{-1}, (s - M_2^2 + i0)^{-1})$. For definiteness, we fix the parameters of the system to values typical for a charmonium system, namely

$$M_1 = 1 \text{ GeV}, \quad M_2 = 3 \text{ GeV}, \quad m = 1 \text{ GeV}, \qquad (13)$$

that ensures that the elastic threshold is located between the bare resonances, $M_1 < 2m < M_2$. Also, for simplicity, we set $g = g_1 = g_2$.

If the loop operator Π is assumed to be constant, the poles can be found analytically in the form

$$s_p = \frac{1}{2}\left(M_1^2 + M_2^2\right) + g^2\Pi \pm \sqrt{\frac{1}{4}\left(M_1^2 - M_2^2\right)^2 + \left(g^2\Pi\right)^2}. \qquad (14)$$

As before, we are interested in the behavior of the poles as the coupling g grows. The picture becomes especially simple, if Π is purely imaginary (for definiteness we set $\Pi = i$). In this case and in the limit $g \to \infty$ the poles given in Eq. (14) become

$$s_p^{(1)} = \frac{1}{2}\left(M_1^2 + M_2^2\right) + 2ig^2 \quad \text{and}$$
$$s_p^{(2)} = \frac{1}{2}\left(M_1^2 + M_2^2\right) - \frac{i}{2g^2}\left(M_2^2 - M_1^2\right)^2, \qquad (15)$$

so that they demonstrate the pattern depicted in Fig. 4(a): One pole acquires a large imaginary part and leaves the near-threshold region fast while the other pole gradually approaches the real axis, that is it becomes nearly stable. The relevant scale for its width is now given by the level spacing $M_2^2 - M_1^2$.

As the loop operator Π acquires a real part (for illustration we set $\Pi = 1 + i$—see Fig. 4(b)), the particular picture changes, however it still demonstrates the same pattern: as the coupling g grows, one state gets stable again while the other one becomes very broad.

Finally, we study the interplay of the different phenomena discussed in this Section. We consider the energy-dependent loop operator $\Pi(s)$ as given in Eq. (5) and fix the Δ-term in the form

$$\Delta = \frac{1}{32\pi m}\sqrt{4m^2 - M_1^2}\,, \qquad (16)$$

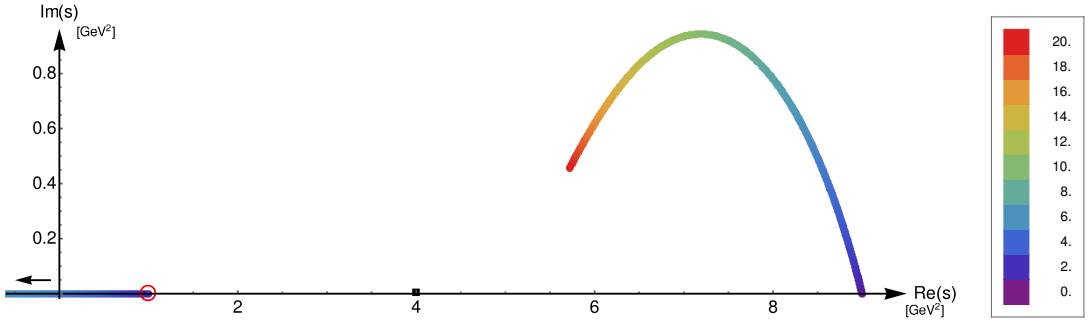

Fig. 5: Pole trajectories in the upper half of the complex s-plane for the energy-dependent loop operator $\Pi(s)$ given by Eq. (5) with the Δ fixed as in Eq. (16). The coupling g is increased from 0 to 20. The black square indicates the threshold while the red circle shows the position of the bound state which is kept constant due to the particular choice of Δ—see Eq. (16).

which ensures that the position of the pole on the first Riemann sheet (the bound-state pole) remains on its location. At the same time its mirror pole on the second Riemann sheet moves away towards smaller and then negative values of s. The results of the corresponding numerical calculations are shown in Fig. 5. In the meantime, the resonance pole (its mirrored counterpart is not shown in Fig. 5) acquires a small width as g departs from 0. However, contrary to naive expectations, it does not become infinitely broad for large values of g. Instead, as g exceeds some critical value the width tends to decrease, so that eventually, for $g \to \infty$, this state tends to decouple from the continuum.

Before we proceed to multi-resonance systems, let us briefly summarize the findings of this Section. On the one hand, using simple and transparent models we found that, contrary to naive expectations, at least one state does not become infinitely broad in the limit of a strong coupling to the hadronic channel—on the contrary, it even decouples from the continuum in this limit thus turning to an asymptotically stable object. In addition, we demonstrated that the renormalization condition for the hadronic loop is an essential ingredient of the model—the form of a particular pole trajectory and whether or not a particular state decouples from the continuum may depend strongly on it. Stated differently: Two different models which are able to describe the physical spectrum of hadrons equally well may predict very different pole trajectories as soon as the coupling constants deviate from their physical values.

4 Unitarization in multi-resonance systems

In the previous Section we studied a single-resonance and a two-resonance system and found that the trajectories of the resonance poles that emerge as the coupling to the continuum is increased depend strongly on both the energy dependence of the selfenergy and on the renormalization condition for the loop. In this Section we consider multi-resonance systems and find the collective phenomena already mentioned above.

4.1 Multi-resonance toy model

To study the coupling of a tower of quark states to a continuum channel, we consider a system governed by the Lagrangian

$$\mathcal{L} = \frac{1}{2}\left[(\partial_\mu\varphi)^2 - m^2\varphi^2\right] + \frac{1}{2}\left[(\partial_\mu\bar{\varphi})^2 - m^2\bar{\varphi}^2\right] + \sum_{n=1}^{N}\left[\frac{1}{2}(\partial_\mu R_n)^2 - \frac{1}{2}M_n^2R_n^2 + g_nR_n\bar{\varphi}\varphi\right], \quad (17)$$

which is a natural generalization of Lagrangian (1) to the multi-resonance case. Here, as before, φ and R_n ($n \in \{1,\ldots,N\}$) are scalar quark-antiquark fields, and $\bar{\varphi}$ is the charge conjugated field with respect to φ. The number of resonance states considered, N, is varied in what follows. It is natural to identify the fields R_n with the n-th radial excitation of the $\bar{Q}Q$ meson, where Q is a heavy quark. Then φ and $\bar{\varphi}$ are heavy-light $\bar{Q}q$ and $\bar{q}Q$ mesons, respectively, produced from R_n through some string breaking mechanism.

The T matrix for $\varphi\bar{\varphi}$ scattering may be written as $T = (1 + V\Pi(s))^{-1}V$, where the potential reads

$$V = \sum_{n=1}^{N} \; ig_n \;\; \underset{R_n}{\text{---}\!\!\!\!\!\!\!\!} \;\; ig_n = -\sum_{n=1}^{N}\frac{g_n^2}{s - M_n^2}. \quad (18)$$

For simplicity, for $\Pi(s)$ we again resort to the scalar loop up to the leading order in k, as defined in Eq. (5). For the masses of the particles R_n we use phenomenological quark models. The results discussed in detail below are based on a model that exhibits a linear confinement potential. Note that we repeated all calculations also with a quadratic confinement potential and found that, while there are differences in the details, the pattern of the level spacing has no influence on the general behavior of the pole trajectories discussed in the paper.

To make things as simple as possible, we consider the large-n limit and approximate the masses M_n as

$$M_n = 2M_Q + E_n, \quad (19)$$

where E_n is the n-th eigenenergy of the massless Hamiltonian

$$H = 2p_r + \sigma r. \tag{20}$$

Here p_r is the radial component of the momentum operator and σ is the string tension. With the help of the quasiclassical quantization condition the eigenspectrum $\{E_n\}$ can be found in a simple analytic form (see, *e.g.*, the discussion in Ref. [35]),

$$E_n^2 = 4\pi\sigma(n-1), \quad n = 1, 2, \ldots, N, \tag{21}$$

where we dropped the zero-point energy such that the energy is counted from the ground state level with energy E_1. We therefore arrive at a very simple analytical formula for the mass spectrum of the resonances R_n,

$$M_n = 2M_Q + \sqrt{4\pi\sigma(n-1)}, \quad n = 1, 2, \ldots, N, \tag{22}$$

which will be used in numerical calculations below. Strictly speaking, approximation (22) can only be used for $n \gg 1$, however, the error we make using Eq. (22) for the states with $n \sim 1$ does not affect the phenomena under study.

In order to proceed we need to specify the parameters of the model. We again stick to values that are phenomenologically adequate in the charm sector,

$$\sigma = 0.16 \text{ GeV}^2, \quad M_Q = 1.7 \text{ GeV}, \quad m = 2 \text{ GeV} \tag{23}$$

for the string tension σ, the heavy-quark mass M_Q, and the mass of the field φ. In particular, $m > M_Q$ complies with the interpretation of the field φ as a heavy-light meson containing the heavy quark Q. Also, for such masses, the $\varphi\bar{\varphi}$ threshold lies at $2m = 4$ GeV while the lowest states R_1 and R_2 have the masses 3.4 GeV and 4.8 GeV, respectively, that is R_1 appears below the threshold while all other R_n's, with $n > 1$, lie above it. This way we can study the behavior of both the bound (virtual) state and the resonances with a varying coupling strength.

For the last parameters of Lagrangian (17)—namely, for the coupling constants g_n—we consider two models. As Model A we employ the simplest assumption on the behavior of the coupling constants g_n and treat them as energy- and n-independent constants. Therefore, in model A we use

$$\text{Model A}: \quad g_n = g \tag{24}$$

for all values of n. In Subsec. 4.4 we repeat our analysis for another model for the couplings g_n and arrive at essentially the same conclusions.

4.2 Pole trajectories and the impact of renormalization

It was argued and illustrated in the previous Section that the renormalization condition strongly affects the pole trajectories. Now we come to a systematic study of this effect in multi-resonance systems which allows us to identify a new phenomenon related to a collective behavior of the poles. To this end we use the toy model described above and stick to Model A for the couplings—see Eqs. (17) and (24), respectively.

We start considering a multi-resonance model (17) with $N \gg 1$—for illustration we stick to $N = 10$ and $N = 20$—and use three different ways to fix the Δ-term in the loop operator defined in Eq. (5) (to understand the origin of this freedom we refer the reader to the discussion below Eq. (5)):

(i) we keep the bound state fixed in its original position (*cf.* Eq. (16));
(ii) we choose $\Delta = 0$—this condition may be understood as absorbing the real part of the loop into the masses of the resonance states;
(iii) we set $\Delta = -0.1$ to illustrate better the impact of the renormalization condition on the pole trajectories.

Trajectories of the poles for cases (i), (ii), and (iii) above are shown in Figs. 6, 7, and 8, respectively. One can draw several conclusions from these figures. To begin with, the poles show the same behavior as in the simple examples from the previous Section. For $g = 0$ there are two degenerate poles below the threshold, located at $s = M_1^2$, one on the first sheet (bound state) and one of the second sheet (virtual state), and, in addition, there are pairs of poles on the second sheet at $s = M_n^2$ $(n > 1)$. For the coupling g departing from 0 the latter poles with $n > 1$ acquire imaginary parts which, for small values of g, grow with increasing values of g. However, as the coupling exceeds some critical value, the pole trajectories bend and start to approach the real axis again. As a result, the resonances decouple from the continuum for large values of g.

Meanwhile, the behavior of the poles for $n = 1$ deserve special attention. The fate of the bound state pole and its virtual mirror state depends strongly on the assumption made for the subtraction term Δ. For example, in case (i) the virtual state goes far away from the threshold as g grows while in case (iii) the virtual level and the bound state have nearly equal masses for all values of the coupling.

In addition, some of the resonance poles with $n > 1$ demonstrate a striking behavior—see Figs. 6-8. In case (i) all resonance trajectories look similar and the poles behave as was just explained above. However the $n = 2$ trajectory hits the real axis just below the threshold thus producing two virtual states of which one proceeds toward the threshold along the real axis. In the meantime, in case (ii), the trajectory with $n = 6$ deviates severely from the "normal" behavior. Indeed, this state acquires a far larger width compared to the other resonances before it turns around. Also, its real part spans a far wider range. In the last case, (iii), an unusual behavior is exhibited by the highest state with $n = 10$.

The result reported in this Section are obtained for the scalar loop taken to leading order in the center-of-mass momentum. If the full expression for the relativistic scalar loop is used instead, an additional nonanalyticity appears on the unphysical sheet and consequently the trajectories change quantitatively. However, qualitatively we observe the same phenomena and thus the conclusions stay unchanged.

To better understand the physics underlying the nontrivial behavior described above, in the next Section we

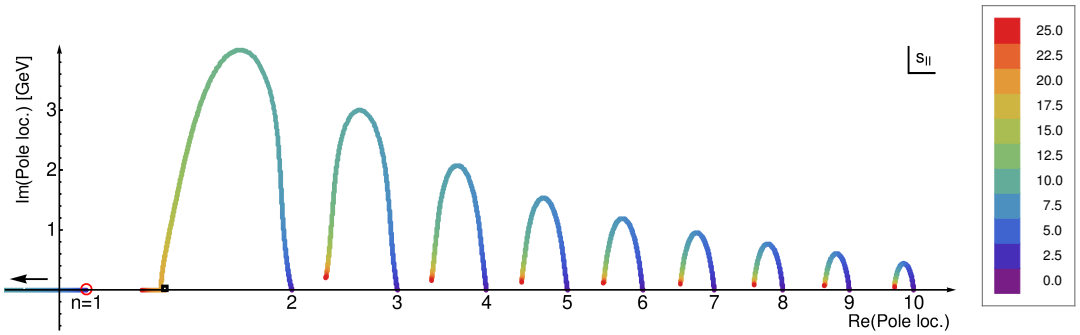

Fig. 6: Pole trajectories in the second Riemann sheet of the complex s-plane for a 10-level system complying with Model A—see Eq. (24)—for the values of g increasing from 0 to 25 GeV. The Δ-term is fixed according to Eq. (16) ($\Delta \approx 0.01$). The black square indicates the position of the threshold. The red circle indicates the position of the bound state on the first sheet. Each trajectory is labeled by their respective principal quantum number n at $g = 0$.

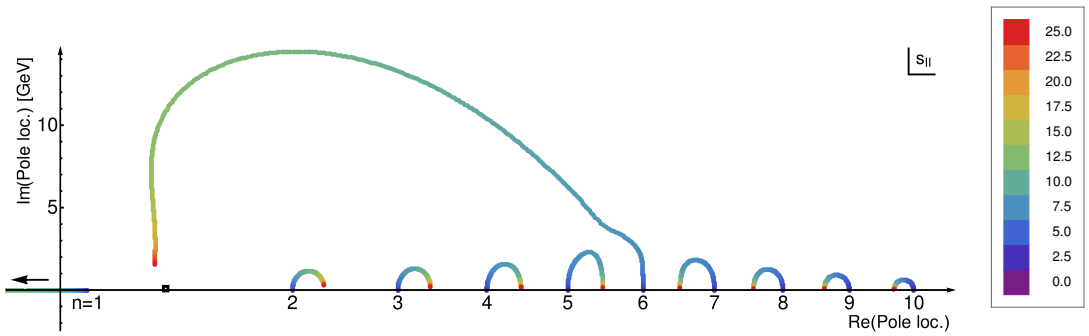

Fig. 7: The same as in Fig. 6 but for $\Delta = 0$.

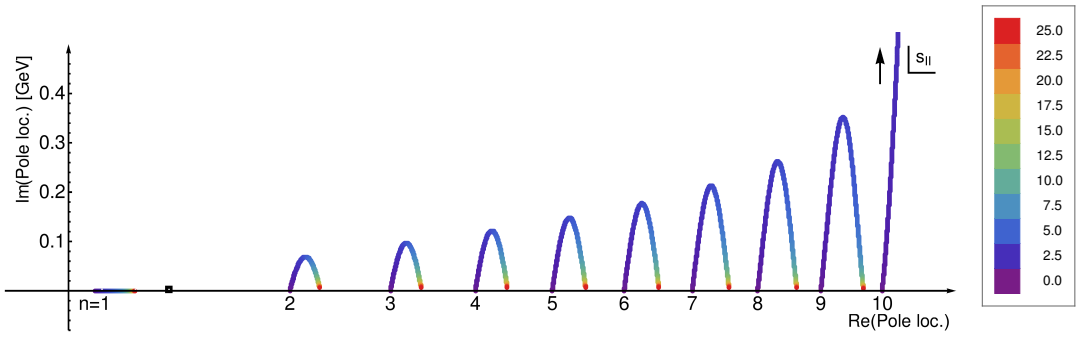

Fig. 8: The same as in Fig. 6 but for $\Delta = -0.1$.

study the residues of the physical propagators of the field R_n.

4.3 Residues and collective phenomena

To better understand the physics behind the trajectories reported above, it is instructive to investigate the residues of the T-matrix poles $\mathcal{R}_i$ where $s_p^{(i)}$ is the i-th pole position. These can be written in the form

$$\mathcal{R}_i = Res\left(T(s_p^{(i)})\right) = \sum_{n,m} g_n g_{n'} Z^{(i)}_{nn'}, \qquad (25)$$

where the field renormalization factors $Z^{(i)}_{nn'}$ were introduced. Since we shall always focus on a particular pole, from now on we drop index i for simplicity.

The propagators of the physical states are given by the solutions of the matrix Dyson equation

$$\mathcal{G}_{nn'}(s) = \delta_{nn'} G_n(s) + \sum_k G_n(s) g_n \Pi(s) g_k \mathcal{G}_{kn'}(s), \qquad (26)$$

where $G_n(s) = (s - M_n^2 + i0)^{-1}$ and the explicit form of the scalar loop, $\Pi(s)$, is given to leading order in the meson

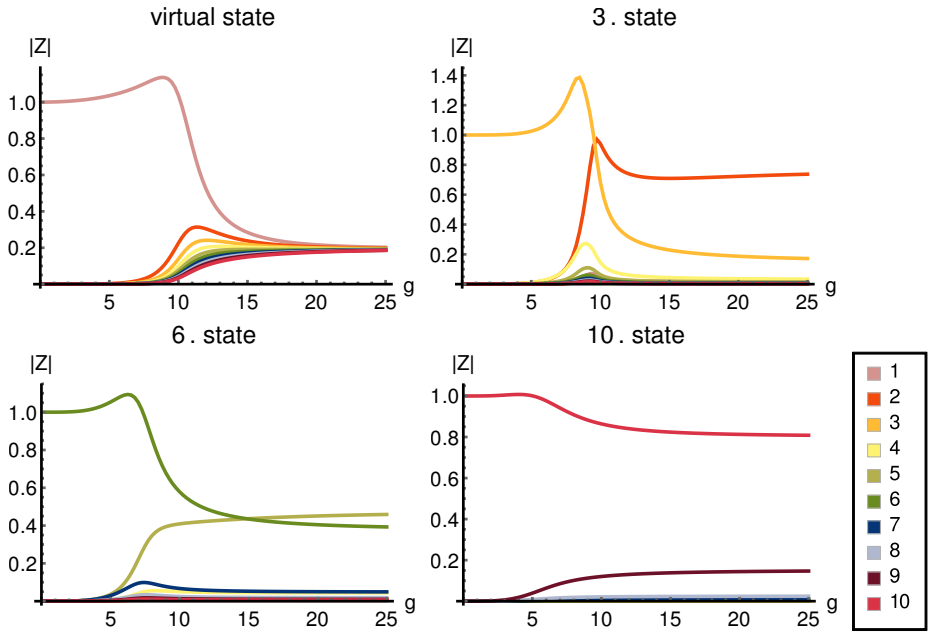

Fig. 9: Absolute values of Z_{nn} for a few resonances for the coupling g growing from 0 to 25 GeV in the 10-level system. The Δ-term is fixed according to Eq. (16) ($\Delta \approx 0.01$).

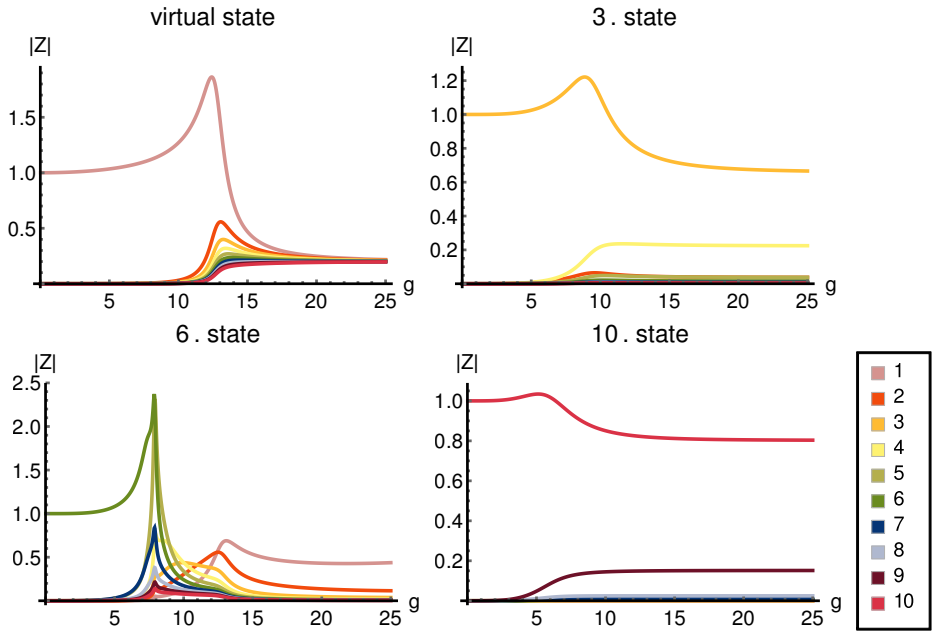

Fig. 10: The same as in Fig. 9 but for $\Delta = 0$.

momentum in Eq. (5). Near the pole s_p one can write term reads

$$\mathcal{G}_{nn'}(s \sim s_p) = \frac{Z_{nn'}}{s - s_p} + \text{regular terms}, \qquad (27)$$

so that $Z_{nn'} = \lim_{s\to s_p}(s - s_p)\mathcal{G}_{nn'}(s)$. Obviously, $s_p = M_n^2$ and $Z_{nn'} = \delta_{nn'}$ for $g = 0$. For nonvanishing couplings g, the solution of the Dyson equation for the n-th diagonal

$$\mathcal{G}_{nn}(s) = \frac{1}{s - M_n^2 - g_n^2 \Pi_n(s)},$$
$$\Pi_n(s) = \frac{1}{\Pi^{-1}(s) - \sum_{k\neq n} g_k^2 G_k(s)}. \qquad (28)$$

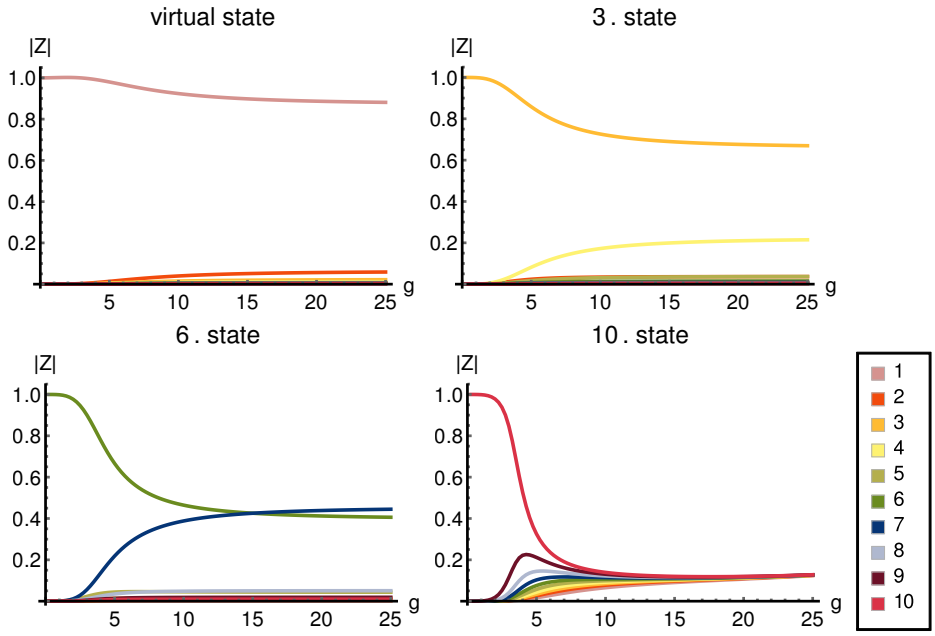

Fig. 11: The same as in Fig. 9 but for $\Delta = -0.1$.

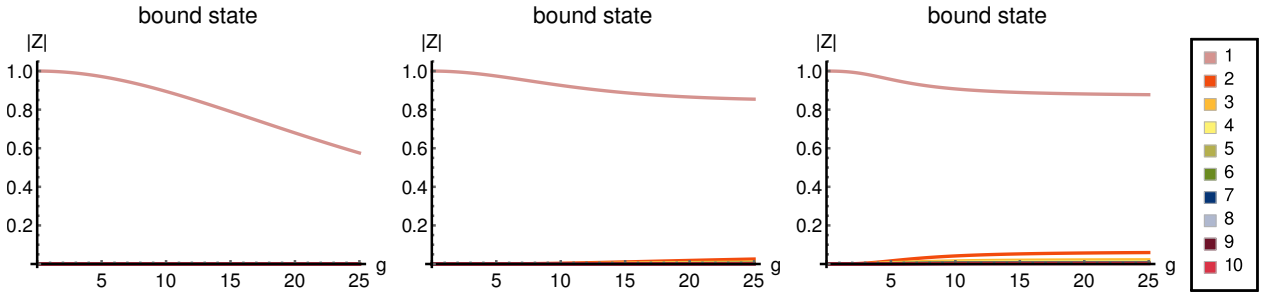

Fig. 12: The same as in Fig. 9 ($\Delta \approx 0.01$), Fig. 10 ($\Delta = 0$) and Fig. 11 ($\Delta = -0.1$) for the bound state.

From this representation one can extract a simple formula for the field renormalization factors (for $s_p \neq M_n^2$),

$$Z_{nn'} = \frac{g_n g_{n'} G_n(s_p) G_{n'}(s_p)}{\sum_k g_k^2 G_k^2(s_p) - \Pi'(s_p)/\Pi^2(s_p)}. \qquad (29)$$

Alternatively those can also be determined numerically.

For a bound-state pole the Z factor takes real values between 0 and 1 and, at least for very near threshold poles, it admits a clear physical interpretation as the probability to observe the bare state in the bound-state wave function [27]. Such a straightforward probabilistic interpretation does not exist for other poles.[4] Nevertheless, in what follows, we look at the absolute values $|Z_{nn}|$ and dare to interpret them, qualitatively and with a lot of caution, as a measure of the admixture of the n-th bare state in the given physical state. In particular, the values of $|Z_{nn}|$ for some representative states are shown in Figs. 9, 10, and 11 for the cases (i), (ii), and (iii), respectively.

[4] Generalizations of the Weinberg approach to coupled channels as well as resonances can be found in Refs. [23,36,37,38,39].

In agreement with the observation of the previous Subsection, Z_{nn} of all poles, but the "abnormal" ones, behave similarly, namely, as the coupling g increases, the given state starts to feel the others, however the influence of the remote states is much weaker than that of the closest neighbors.

Meanwhile, the situation is very different for the unusual states, which feel not only the closest neighbors but typically all the other, more remote states. This kind of collectivity is seen from the behavior of the functions $|Z_{nn}|$ which take comparable values not only for the neighboring poles, but for the remote poles too. This is in line with the observation made in the previous Section that the trajectories of the extraordinary states are not localized and span a wide range.

To complete the picture in Fig. 12 we show the residues for the bound state pole for the different values of Δ employed above. We confirmed that the bound state wave function is properly normalized for all values of g. For the parameter settings used here one can see that the residues are by far dominated by the bare pole that provided the bound state for a vanishing coupling. However, since the

bound state poles are located far below the threshold, an application of the Weinberg criterion to understand the compositeness of the bound state appears not possible. Meanwhile, as discussed above, for cases (i) and (ii) the mirror state in the second sheet (virtual state) is located very asymmetrically presumably pointing at a molecular nature of the bound state according to Ref. [25]. In contrast to this, in case (iii), the virtual state does not move and stays in its original location close to that of the bound state, albeit on the second sheet. Thus, in case (iii) the bound state is indeed to be interpreted as being predominantly a quark state.

To ensure that the observed collective phenomenon is not an artifact of a particular chosen number of poles N we repeat the study outlined above for $N = 20$. For illustration we show the results for the renormalization condition which keeps the bound state mass fixed (case (i)) in Figs. 13 and 14. Clearly the system exhibits exactly the same behavior as discussed before for $N = 10$, namely that some states show a collective behavior for $g \to \infty$ while most of the states tend to decouple from the continuum in this limit.

4.4 Alternative model for the couplings

As the last exercise, in order to demonstrate that our qualitative findings do not depend on the particular model chosen for the couplings, we also use a more realistic model for the vertex functions which we refer to as Model B. To this end we consider the decay of the form $R_n \to \varphi\bar{\varphi}$ and notice that, in order to model the behavior of the coupling g_n, it is sufficient to evaluate the overlap of the wave functions (w.f.s) in the amplitude for the light-quark pair creation through the $^3P_0$ mechanism—for the details see, for example, Refs. [12,41,42,43,44,45,46] and references therein,

$$g_n \propto \int d^3r d^3\rho\, \psi_{R_n}(\boldsymbol{r})\psi^*_{\varphi\bar{\varphi}}(-\boldsymbol{r}/2) \times \psi^*_{\varphi}(\boldsymbol{r}/2+\boldsymbol{\rho})\psi^*_{\bar{\varphi}}(\boldsymbol{r}/2-\boldsymbol{\rho}), \qquad (30)$$

where the standard relative Jacobi coordinates $\boldsymbol{r}$ and $\boldsymbol{\rho}$ are introduced as shown in Fig. 15, ψ_{R_n}, ψ_φ, and $\psi_{\bar{\varphi}}$ are the bound-state w.f.s of all mesons involved, $\psi_{\varphi\bar{\varphi}}(\boldsymbol{r}) = e^{i\boldsymbol{k}\boldsymbol{r}}$ is the w.f. of the free motion of the mesons φ and $\bar{\varphi}$ with the relative momentum $\boldsymbol{k}$, that is $\boldsymbol{P}_\varphi = -\boldsymbol{P}_{\bar{\varphi}} = \boldsymbol{k}$.

The w.f. of the heavy-heavy quarkonium R_n is localized at small interquark separations while the typical size of the heavy-light mesons φ and $\bar{\varphi}$ is much larger. Consequently the mass parameter β_R which governs the falloff of the w.f. ψ_{R_n} with the quark separation is large compared to the corresponding parameter for the meson φ, $\beta_R \gg \beta_\varphi$. As a result the w.f. $\psi_{R_n}(\boldsymbol{r})$ cuts the integral in r at $r \ll \rho$, so that, approximately,

$$g_n \propto \left(\int d^3r e^{-i\boldsymbol{k}\boldsymbol{r}/2}\psi_{R_n}(\boldsymbol{r})\right)\left(\int d^3\rho \psi^*_\varphi(\boldsymbol{\rho})\psi^*_{\bar{\varphi}}(-\boldsymbol{\rho})\right) = \int d^3r e^{-i\boldsymbol{k}\boldsymbol{r}/2}\psi_{R_n}(\boldsymbol{r}) = \Psi_{R_n}(\boldsymbol{k}/2), \qquad (31)$$

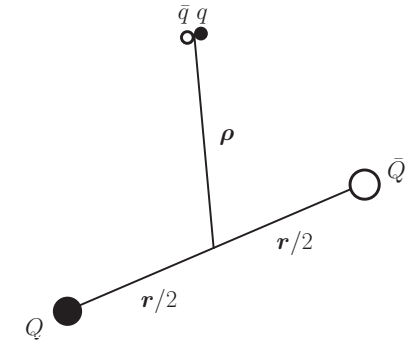

Fig. 15: Graphical representation of the pair creation mechanism.

where Ψ_{R_n} is the Fourier transform of the coordinate w.f. $\psi_{R_n}(\boldsymbol{r})$, and it was used that $\psi^*_{\bar{\varphi}}(-\boldsymbol{\rho}) = \psi_\varphi(\boldsymbol{\rho})$ and that the w.f. $\psi_\varphi(\boldsymbol{\rho})$ is normalized.

If, for simplicity, we stick to the quasiclassical w.f. Ψ_R then it is easy to find that

$$g_n \propto \Psi_{R_n}(\boldsymbol{k}/2) \propto \exp\left(-\frac{k^2}{4\sigma}\right). \qquad (32)$$

In the decay $R_n \to \varphi\bar{\varphi}$ the momentum k is fully fixed by the masses of the particles in the initial and in the final states. On the other hand, in the scattering process $\varphi\bar{\varphi} \to R_n \to \varphi\bar{\varphi}$, k is related to the invariant energy s as given by Eq. (4). Thus, as Model B, we use the form

$$\text{Model B}: \quad g_n = g e^{-\lambda^2 k^2} \qquad (33)$$

which smoothly interpolates between Model A ($\lambda = 0$) and formula (32) with $\lambda = 1/(2\sqrt{\sigma}) = 1.25$ GeV^{-1}. Strictly speaking the approximations used to derive Eq. (33) are valid for low-lying resonances R_n, while for $n \gg 1$ the high-order pre-exponential polynomial in the R_n's w.f. starts to compete with the exponential factor so that Ψ_{R_n} is not short-ranged any more. As a consequence, the overlap of the w.f.s in Eq. (31) acquires a dependence on the excitation number n and so does the coupling g_n from Eq. (33). However, inclusion of this effect goes well beyond the scope of the present work, which is aimed at a qualitative investigation of the unitarization effects on the spectrum of quark states. We therefore leave a more refined treatment of the couplings g_n for future publications and stick here to the simplest form presented in Eq. (33).

The scalar loop for Model B is given by the expression

$$\Pi(s) = \frac{1}{16\pi^2 m}\int_0^\infty \frac{p^2}{k^2-p^2}e^{-\lambda^2 p^2}dp = -\frac{i}{16\pi m}k e^{-\lambda^2 k^2} + \frac{1}{16\pi^2 m}\mathcal{P}\int_0^\infty \frac{p^2}{k^2-p^2}e^{-\lambda^2 p^2}dp, \qquad (34)$$

where $\mathcal{P}$ stands for the principal value prescription. As one can see, different values of λ, referring to different

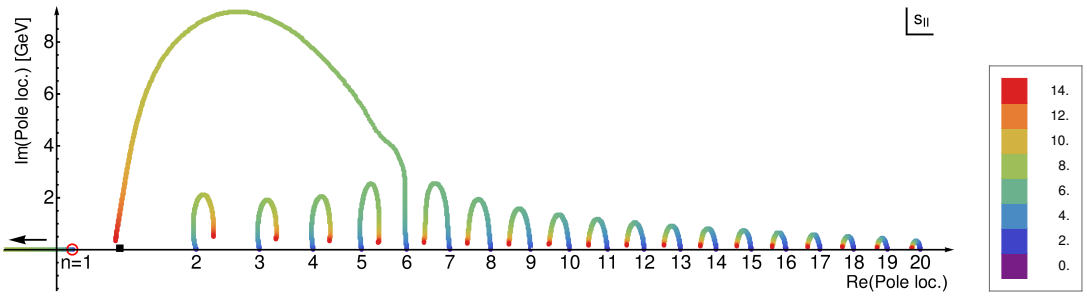

Fig. 13: The same as in Fig. 6 but for $N = 20$.

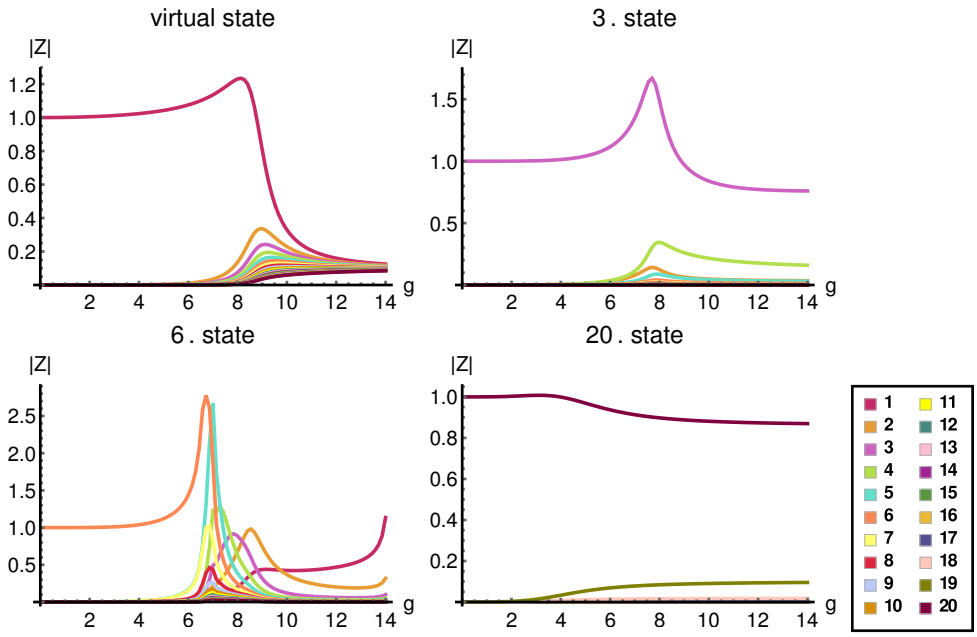

Fig. 14: The same as in Fig. 9 but for $N = 20$. The rise of the $Z_n n$ at $g \to 14$ for the $n = 6$ state is due to a peak which reveals itself when the trajectory hits the real axis. Such effects were also observed before—see, for example, Ref. [40].

quark models, provide different values of the real part of the loop and, when parametrized in the form of Eq. (5), correspond to different values of Δ.

In Fig. 16 we plot the pole trajectories for Model B with $N = 10$ and with $\lambda = 0.1$ GeV^{-1}, 0.3 GeV^{-1}, and 0.7 GeV^{-1}, respectively. From these figures one can see that Model B demonstrates essentially the same pattern as Model A. We refrain from considering larger values of λ as spurious poles start to appear in this case on both the unphysical and sometimes even on the physical sheet. For large values of the coupling g these poles tend to approach the physical region and to interfere with the physical poles. This would make an interpretation of the latter questionable. Such spurious poles are artifacts of the particular parametrization used for the vertex function. Building a more reliable parametrization should solve the problem, however, this goes beyond the scope of the present paper.

5 Interpretation

In this paper we found the following universal features which emerge when quark states get coupled to the continuum in a way consistent with unitarity, once the coupling gets too large to be treated perturbatively:

- As soon as the selfenergies get of the order of the level spacing, for most states the pole trajectories bend and the width decreases again. These states are mostly influenced by their nearest neighbors.
- Besides the states just described at least one state possesses a pole trajectory which spans a wide (compared to the level spacing) range therefore acquiring contributions from multiple bare poles—we therefore call it a collective state.
- Which state shows this collective phenomenon and if this collectivity shows up in one or more states depends on the renormalization condition imposed and on the details of the model.

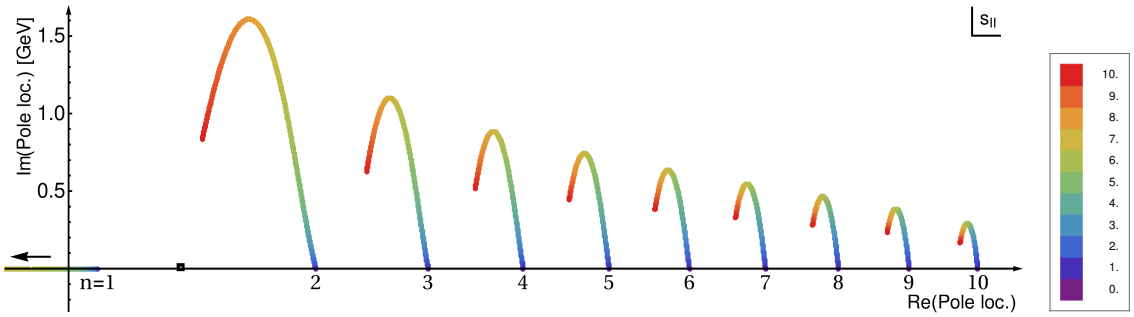

(a) $\lambda = 0.1$ GeV^{-1}

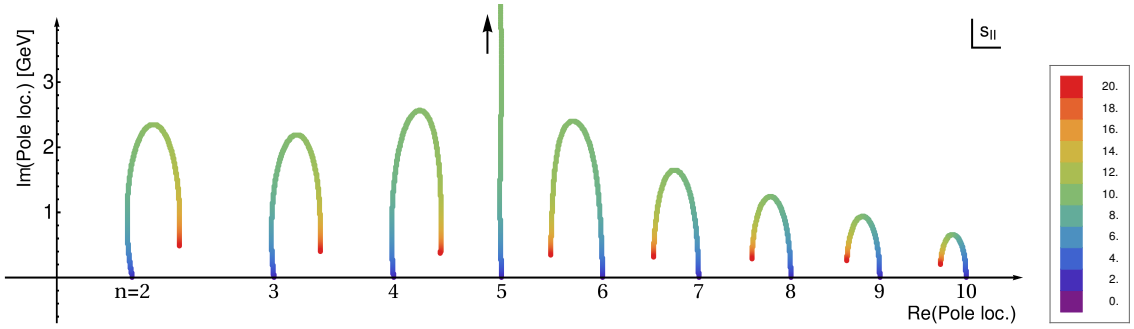

(b) $\lambda = 0.3$ GeV^{-1}

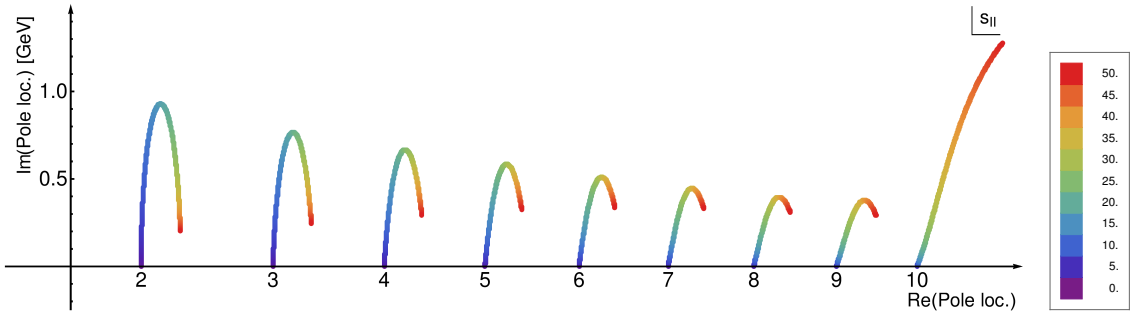

(c) $\lambda = 0.7$ GeV^{-1}

Fig. 16: Pole trajectories in the complex s-plane for Model B with different values of λ. The black square indicates the threshold.

Clearly, to study the evolution of a collective pole as a function of some strength parameter, it is not sufficient to start from a reduced basis since in this case one omits states that are of relevance for the collective one. This does not mean, however, that it is not possible to build an effective theory with only a few states for a given physical situation—one only has to question the applicability of the same effective description when the strength parameter is varied over a large range.

The observation of the collective states could remind one of the notion of duality—for a detailed review on the subject see, for example, Refs. [47,48]—which can be formulated as the observation that an infinite sum of s-channel poles can be matched onto an infinite sum of t-channel poles—this relation is illustrated in Fig. 17. This might explain why it was possible to predict, for example, the existence of $X(3872)$ charmoniumlike state from simple meson exchange models [49,50,51]. The extraordinary states found here appear as a collective phenomenon of basically all s-channel pole terms included in the model, and one might be tempted to claim that this would still be true even if infinitely many states were included. Then one could argue, based on the duality picture, that the very same pole could have emerged from an infinite sum of t-channel poles and that it might well be more efficient to parametrize the binding potential by a contact term or a few t-channel exchanges instead of a large sum of s-channel poles.

6 Summary and Outlook

Within different quark models we studied the trajectories of series of S-matrix poles as their coupling to a continuum channel is increased from 0 to some large value while

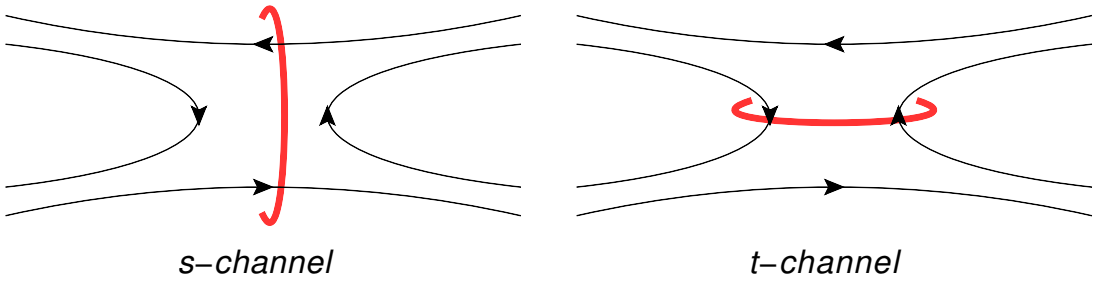

Fig. 17: An illustration of the duality idea: a given quark-model diagram can either be viewed as a s-channel exchange or a t-channel exchange depending on which interaction produces a pole. Here the two possible clusterings are indicated by the red lines.

keeping other input parameters fixed. As outlined in the Introduction, such a study could be understood as a naive implementation of the behavior of the QCD spectrum as the number of colors is reduced from some very large value.

In this work we varied the confining potential, the vertex functions as well as the number of quark states included and found that the qualitative features of the pole trajectories persisted. Although all models used were quite simple (*e.g.* no vertex dressing via t-channel meson exchange was involved) we still expect that the gross features described in this paper are genuine and should appear in all models where the couplings of s-channel resonances to continuum states are varied over a wide range. Especially one is to conclude that, when unitarizing a quark model, care has to be taken with respect to the renormalization condition imposed for the hadronic loops. Indeed, the way how the hadronic loops are regularized within that model provides effectively a modeling for the quantity Δ discussed in this paper (*cf.* Eq. (5)) which strongly influences the pole trajectories. Stated differently: the pole trajectories of quark model states as a function of some coupling have to be interpreted with caution since one gets sensitive to the regularization imposed for the hadronic loops, that is to an effect which might lie beyond the scope of the quark model itself. As a result, the mentioned trajectories might come out as artifacts (for additional aspects about unitarizing the quark model we refer the reader to Ref. [52]).

Another important insight is that, when quark states couple strongly to the continuum, at least one state develops an extraordinary, collective nature. The collectivity found here might be interpreted as the onset of effectively building a t-channel exchange from an infinite sum of s-channel poles. In this sense the extraordinary states might come out as hadronic molecules, at least when they are located near relevant thresholds.

In the models studied in this paper we witnessed the appearance of one or two such extraordinary states depending on the renormalization condition. However, for simplicity we limited ourselves to the study of only one continuum channel. To gain insight into the physics of heavy mesons a natural next step is the inclusion of more channels. First investigations indicate that the number of collective states tends to increase in this case.

For the selfenergies in this work we only used the expression for the scalar loop in leading order in the meson–meson relative momentum. As a result of this the number of poles in the S matrix stayed the same throughout the study, at least for model A. If instead the full expression for the relativistic scalar loop had been used, there would have appeared an additional nonanalyticity on the second sheet that leads to an additional pole. As a result the trajectories change quantitatively. However qualitatively they stay the same and so do the conclusions on the ordinary and extraordinary nature of the resonances as well as on the role played by the renormalization scheme. Further details will be presented elsewhere.

The authors are grateful for useful discussions with E. Eichten, J. Gegelia, F.-K. Guo, U.-G. Meißner, Yu. S. Kalashnikova, A. E. Kudryavtsev, and A. Wirzba. This work is supported in part by the DFG and the NSFC through funds provided to the Sino-German CRC 110 “Symmetries and the Emergence of Structure in QCD” (NSFC Grant No. 11261130311). AVN acknowledges support from the Russian Science Foundation (Grant No. 15-12-30014).

References

1. T. Barnes and E. S. Swanson, Phys. Rev. C **77** (2008) 055206.
2. E. van Beveren, C. Dullemond and G. Rupp, Phys. Rev. D **21** (1980) 772 Erratum: [Phys. Rev. D **22** (1980) 787].
3. N. A. Tornqvist and M. Roos, Phys. Rev. Lett. **76** (1996) 1575.
4. M. Boglione and M. R. Pennington, Phys. Rev. Lett. **79** (1997) 1998.
5. E. van Beveren and G. Rupp, Int. J. Theor. Phys. Group Theor. Nonlin. Opt. **11** (2006) 179.
6. E. van Beveren, D. V. Bugg, F. Kleefeld, and G. Rupp, Phys. Lett. B **641** (2006) 265.
7. E. van Beveren and G. Rupp, Annals Phys. **324** (2009) 1620.
8. G. Rupp, E. van Beveren, and S. Coito, Acta Phys. Polon. Supp. **8** (2015) 139.
9. G. Rupp, S. Coito, and E. van Beveren, Acta Phys. Polon. Supp. **5** (2012) 1007.
10. T. Wolkanowski, F. Giacosa, and D. H. Rischke, Phys. Rev. D **93** (2016) 014002.

11. B. O. Kerbikov, V. G. Ksenzov, A. E. Kudryavtsev, V. E. Markushin and I. S. Shapiro, ITEP preprint No. 61 (1978).
12. E. Eichten, K. Gottfried, T. Kinoshita, K. D. Lane, and T. M. Yan, Phys. Rev. D **17** (1978) 3090; Erratum: [Phys. Rev. D **21** (1980) 313].
13. P. G. Ortega, J. Segovia, D. R. Entem and F. Fernandez, Phys. Rev. D **81** (2010) 054023.
14. D. R. Entem, P. G. Ortega and F. Fernandez, AIP Conf. Proc. **1735** (2016) 060006.
15. E. Cincioglu, J. Nieves, A. Ozpineci and A. U. Yilmazer, arXiv:1606.03239 [hep-ph].
16. G. 't Hooft, Nucl. Phys. B **72** (1974) 461.
17. E. Witten, Annals Phys. **128** (1980) 363.
18. J. F. Donoghue, E. Golowich and B. R. Holstein, Camb. Monogr. Part. Phys. Nucl. Phys. Cosmol. **2** (1992) 1, (Second Edition, 2014).
19. J. R. Pelaez, arXiv:1510.00653 [hep-ph].
20. R. L. Jaffe, AIP Conf. Proc. **964** (2007) 1 [Prog. Theor. Phys. Suppl. **168** (2007) 127].
21. J. Schneitzer, T. Wolkanowski and F. Giacosa, Nucl. Phys. B **888** (2014) 287.
22. L. N. Bogdanova, G. M. Hale and V. E. Markushin, Phys. Rev. C **44** (1991) 1289.
23. V. Baru, J. Haidenbauer, C. Hanhart, Yu. Kalashnikova, and A. E. Kudryavtsev, Phys. Lett. B **586**, 53 (2004).
24. F. Giacosa and G. Pagliara, Phys. Rev. C **76** (2007) 065204.
25. D. Morgan, Nucl. Phys. A **543**, 632 (1992).
26. N. A. Tornqvist, Phys. Rev. D **51**, 5312 (1995).
27. S. Weinberg, Phys. Rev. **130**, 776 (1963).
28. C. Hanhart, J. R. Pelaez, and G. Rios, Phys. Lett. B **739** (2014) 375.
29. V. Baru, C. Hanhart, Y. S. Kalashnikova, A. E. Kudryavtsev and A. V. Nefediev, Eur. Phys. J. A **44** (2010) 93.
30. C. Hanhart, Y. S. Kalashnikova and A. V. Nefediev, Eur. Phys. J. A **47** (2011) 101.
31. F.-K. Guo, C. Hanhart, Yu. S. Kalashnikova, P. Matuschek, R. V. Mizuk, A. V. Nefediev, Q. Wang, and J.-L. Wynen, Phys. Rev. D **93** (2016), 074031.
32. Yu. S. Kalashnikova, Phys. Rev. D **72** (2005) 034010.
33. I. V. Danilkin and Yu. A. Simonov, Phys. Rev. D **81** (2010) 074027.
34. I. V. Danilkin and Yu. A. Simonov, Phys. Rev. Lett. **105** (2010) 102002.
35. Yu. S. Kalashnikova, A. V. Nefediev, and Yu. A. Simonov, Phys. Rev. D **64** (2001) 014037.
36. T. Hyodo, Int. J. Mod. Phys. A **28** (2013) 1330045.
37. T. Sekihara, T. Hyodo and D. Jido, PTEP **2015** (2015) 063D04.
38. F. Aceti, L. R. Dai, L. S. Geng, E. Oset and Y. Zhang, Int. J. Mod. Phys. Conf. Ser. **26** (2014) 1460077.
39. Z. H. Guo and J. A. Oller, Phys. Rev. D **93** (2016), 096001.
40. J. Nebreda and J. R. Pelaez, Phys. Rev. D **81** (2010) 054035.
41. P. Geiger and E. S. Swanson, Phys. Rev. D **50** (1994) 6855.
42. E. S. Ackleh, T. Barnes, and E. S. Swanson, Phys. Rev. D **54** (1996) 6811.
43. J. F. Liu and G. J. Ding, Eur. Phys. J. C **72** (2012) 1981.
44. J. Ferretti, G. Galata, E. Santopinto and A. Vassallo, Phys. Rev. C **86** (2012) 015204.
45. J. Ferretti and E. Santopinto, Phys. Rev. D **90** (2014) 094022.
46. Y. Lu, M. N. Anwar and B. S. Zou, arXiv:1606.06927 [hep-ph].
47. M. Fukugita and K. Igi, Phys. Rept. **31** (1977) 237.
48. M. A. Shifman, in *At the Frontier of Particle Physics*, edited by M. Shifman, Vol. 3 (World Scientific, 2001) pp. 1447-1494.
49. M. B. Voloshin and L. B. Okun, JETP Lett. **23** (1976) 333 [Pisma Zh. Eksp. Teor. Fiz. **23** (1976) 369].
50. A. De Rujula, H. Georgi, and S. L. Glashow, Phys. Rev. Lett. **38** (1977) 317.
51. N. A. Tornqvist, Phys. Rev. Lett. **67** (1991) 556.
52. S. Capstick *et al.*, Eur. Phys. J. A **35** (2008) 253.